 doi:10.20944/preprints202002.0333.v1

Article

Diurnal Cycle of Convection over Lake Titicaca Basin based on the Satellite Data from the Climate Prediction Center Morphing (CMORPH)

Eleazar Chuchón Angulo [1], Augusto Jose Pereira Filho [2]

[1,2] Institute of Astronomy, Geophysics and Atmospheric Sciences, University of Sao Paulo, Sao Paulo, Brazil, eleazar.angulo@alumni.usp.br, augusto.pereira@iag.usp.br

* Correspondence: eleazar.angulo@alumni.usp.br; Tel.: +55-11-3091-2851

Abstract: This paper examines the diurnal cycle of convection (DCC) over Lake Titicaca Basin (LTb) during summertime months based on the high spatial resolution (8 x 8 km^2) and hourly temporal resolution, estimates of Climate Prediction Center Morphing technique (CMORPH). Analysis was performed using observed data from rain gauges (Rg-SENAMHI) for the period 2002 to 2013. Graphical comparisons and several statistical metrics such as correlation coefficient, bias, and root mean square error were used to evaluate CMORPH product. Spatial maps and graphic metrics of diurnal cycle were developed to assess CMORPH data, spatial dependency an accuracy over the LTb. Approximately, 43% of the total Rg-SENAMHI variation is explained CMORPH data. The correlation between Rg-SENAMHI and CMORPH is positively over southeast and northern LTb, and negatively in the central and southern LTb. A underestimation bias is observed over most the LTb areas and overestimation bias (e.g., Lagunillas, Isla Suana and Desaguadero stations). In general, spatial patterns of rainfall over the LTb were captured through CMORPH data. Over the surrounding lake area, high mountain, and plateau area, maximum peaks of precipitation occur in the early evening, neverhtheless over low areas such as the lake, surrounding and valleys, maximum precipitation values occur early morning. The results show that DCC its very related by surface exchange processes and local circulation resulting from solar radiation and heterogeneous topography.

Keywords: CMORPH; Diurnal cycle; Titicaca Lake basin

1. Introduction

The precipitation is of great importance in the water cycle. Particulary, understand rainfall spatial-temporal distribution it is going to help a lot in the livelihood of the many Lake Titicaca basin (LTb) communities that predominantly rely on rain fed agriculture [1]. Today, to observe and estimate the amount of surface rain, there are many methods such as rain gauges, satellite sensors and radars. A direct way to measure the rainfall is it through the rain gauges, but the spatial coverage in the LTb is quite deficient and with unequal spatial distribution. In consequence, extrapolation of precipitation leads to inaccuracies in this conditions [2,3].On the other hand, the meteorological radar is an alternative but due to difficult accessibility of the site, the mountain barriers and the financial limitations the installation of radars is not feasible. For these reasons, satellite sensors is a viable option to assess the rainfall in this region [3,7,12,13].

Many studies have compared, on different scales, the performance between observed and estimated surface rainfall [3-14]. The results show that using different space scales and timescales and indicators it is possible to evaluate whether the efficiency of satellite data varies with the evaluation method, time window and location [2,10,12,13]. The diurnal cycle of precipitation, mainly

at low latitudes, has been analyzed from satellite observations as document in both initial and current works [5,14-27]. These previous studies showed that diurnal variations in precipitation indicate larger amplitudes over land areas than over the oceans during warm seasons. This demostrates that precipitation peak over land areas occurs more frequently during the afternoon, while maximum values of rain over the oceans occur from midnight to early morning [5,14,19,21,25,27].

As is known, the LTb topography features and complex land-lake surface processes have influence the spatial-temporal rainfall distribution over this region [28]. During summertime (December-February) approximately 70% of annual rainfall occurs [28,29,30] with a north-south distribution. Varying from 1400 mm in the north-east to 200 mm in the south-west of the basin [28,31]. Inhomogeneous precipitation in this region can easily result in either major droughts[32] or disastrous flooding [33]. Using nine satellite rainfall estimations [12], found a stronger gradient from north to south and weaker from east to west gradient for the present study region. To our area of interest, exist four published works on the performance of satellite rainfall estimations [12,13,34,35], most of the previous studies focused on the evaluation at the annual, monthly and daily time steps showing high accuracy in dry and relatively flat regions [12,36]. However, there are not studies related to the behavior of the diurnal cycle at the hourly level based in satellite estimates in this region. Studies conducted in other regions of the world shows the ability of CMORPH (Climate prediction centre MORPHing) [37,38] in represent the diurnal cycle of precipitation at the hourly temporal resolution [5,10,14,39-44] and good performance in mountainous regions [6,11,12,14,41,44]. Our study analyses the diurnal cycle of convection over Lake Titicaca basin from on high spatio-temporal resolution data from CMORPH for the period from 2002 to 2013. The document is organized as follows: in sections 2 and 3, we presented methods and data used in this study. In section 4, we comparated between CMORPH and observerd data and discuss the results taking into account terrain complex and lake influenced the diurnal cycle of covection. The conclusions are presented in section 5.

2. Study area and data sets

2.1. Study area

Titicaca Lake is located quite high in the Andes (15°45'56''S and 69°31'34''W), in a geographical area of high plateau morphology, with maximum altitude about 6500 m asl, the total area of the lake is close to 8,400.00 km^2 and storing a volume of 932 km^3 (~3810 m asl). It is surrounded by the eastern and western ranges in the Andes, and the drainage is part of a great fluvial system (TDPS), integrated with the basins Poopó, Coipasa, and Uyuni, all of which have acommon collector in Lake Titicaca [45]. The ratio between the basin area and lake surface is nearly 7:1. The maximum depth of Late Titicaca is 280 m and, its average depth ranges from 140 m to 180 m . Titicaca is known as the largest and highest navigatin lake in South America, with a few commercial boats running from southeastern to northwestern parts of the lake, between cities of Puno (Peru) and to the direction of La Paz city (Bolivia). The tributaries rivers to Lake Titicaca contribute between 201 m^3s^{-1} to 270 m^3s^{-1} of the total annual flow and, its main contribution is mostly from rainfall of convective origin on the lake. Desaguadero River during its course receives water from several tributaries has a mean annual flow of 89 m^3s^{-1} and continues its trajectory to the south until reaching Lake Poopó [46]. The lake is supplied by rainfall (47%) and river water (35%), mainly by the river Ramis and loses water by evaporation (91%) and at the control point in the Desaguadero River (9%), the average annual temperature in the lake basin fluctuates between 7 and 10 ° C [47]. We are mainly interested in the area between 14–18°S and 69–71°W with has an average elevation of 4000 m (Fig. 1)

Preprints (www.preprints.org) | NOT PEER-REVIEWED | Posted: 23 February 2020 doi:10.20944/preprints202002.0333.v1

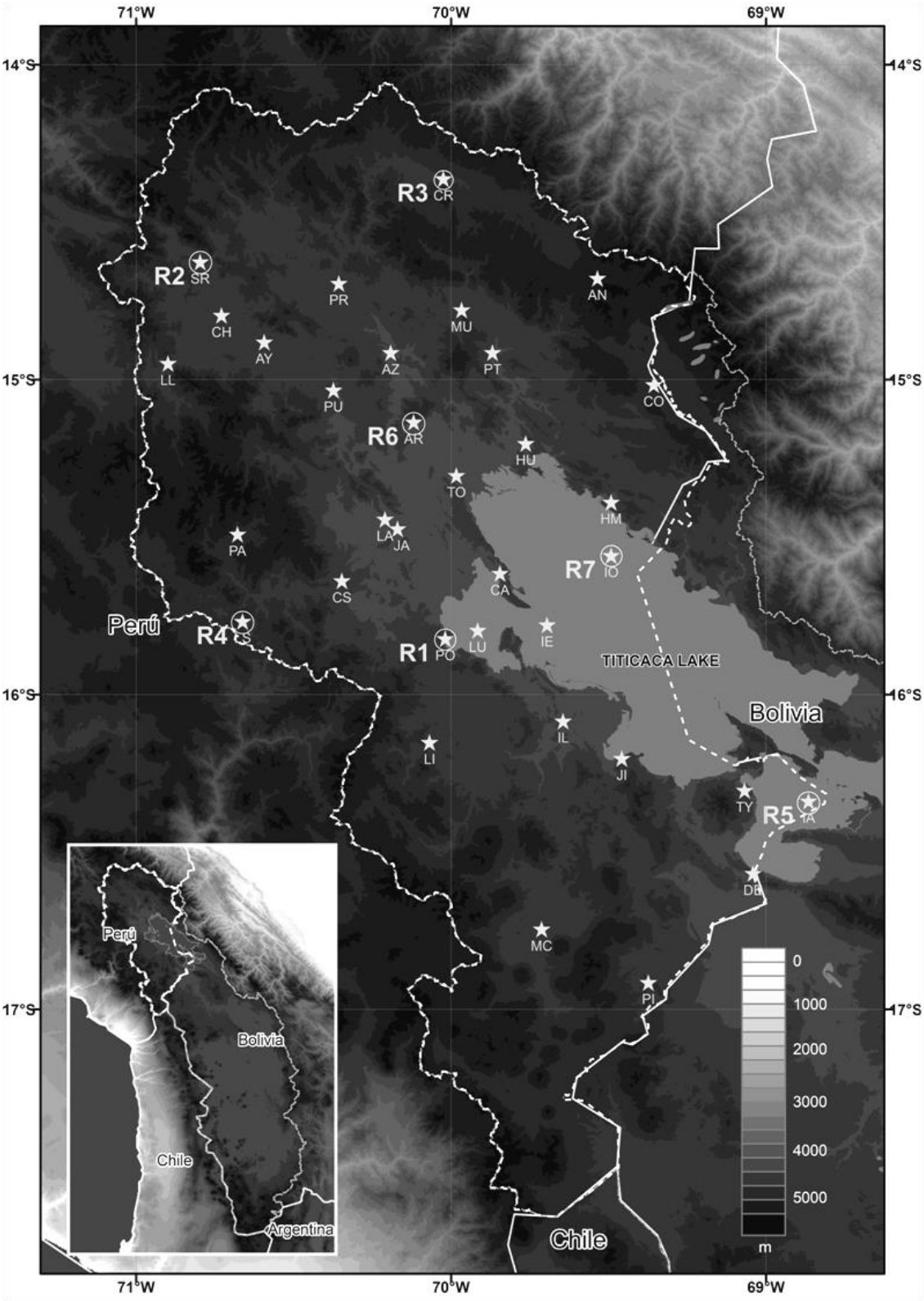

Figure 1. Lake Titicaca Basin, Peru, showing distributions of rain gauges stations. The shaded scale represents terrain elevation. The circles represent the sub-regions studied: Region 1-Puno (70° 01'18 - 69°44'55W, 15°58'28 - 15°43'13S); Region 2-Santa Rosa (70°53'20 - 70°33'54W, 14°39'35 - 14°58'15S); Region 3-Crucero (70°03'47 - 69°46'15W, 14°31'12 - 14°47'35S); Region 4-Cabanillas (70°46'05 - 70°27'02W, 15°34'51 - 15°53'31S); Region 5-Isla Suana (68°59'27 - 68°39'56W, 16°13'59 - 16°33'32S); Region 6-Arapa (70°12'32 - 69°55'16W, 15°05'02 - 15°21'56S); Region 7-Isla Soto (68°28'43 - 69°10'49W, 15°38'39 - 15°55'48S).

Preprints (www.preprints.org) | NOT PEER-REVIEWED | Posted: 23 February 2020 doi:10.20944/preprints202002.0333.v1

2.2. Data set

The rain gauges data sets and satellite used for this study are presented in Table 1, they include rainfall gauge data sets derived from the National Meteorological and Hydrological Service of Peru (Rg-SENAMHI) and CMORPH respectively. We used the period between 2002 and 2013 to do the analysis.

2.2. 1. Gauge precipitation data

The dataset used is result DECADE project (Data on climate and Extreme weather for the Central AnDEs), based in [48] and includes daily precipitation (mm), maximum and minimum temperature (**°C**) measurements, data that previously received statistical control. A total of 34 conventional weather stations and two automatic weather stations were available for this study (Fig. 1). We selected 34 stations with available daily precipitation data (period 2002-2013) of Rg-SENAMHI. Figure 2 shows the monthly precipitation values at the stations located in the Lake Titicaca basin. Annual precipitation average to long-term varies range to 530 mm year^{-1} and 980 mm year^{-1} for the period analysed 2002 to 2013. Almost 82% rainfall annual occurs between November and March months.

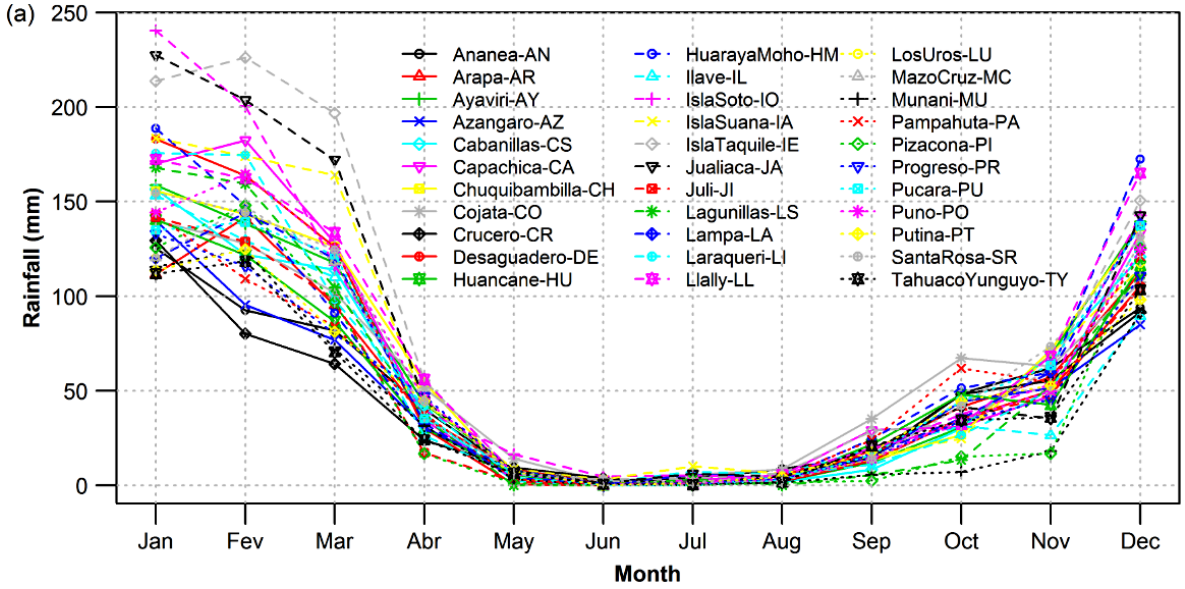

Figure 2. (a) Annual variation of monthly averages of precipitation stations located into Lake Titicaca basin (period 2002 to 2013).

2.2. 2. CMORPH

CMORPH is a precipitation dataset analyses technique described by [35] that uses microwave observation data from several satellites combined with geostationary infrared data, and developed by NOAA's that provides high spatial-temporal resolution (8-km in the equatorial zone and 30-minute) this will allow in-depth understand the diurnal cycle of convection in LTb.

3. Methods

Spatial-temporal CMORPH rainfall estimation is will be linked to the Rg-SENAMHI rainfall observed as follows:

In the firts way (point-to-grid comparison) CMORPH and Rg-SENAMHI dataset are compared within the satellite grid box. This first test establishes that locally observerd are compared with

Preprints (www.preprints.org) | NOT PEER-REVIEWED | Posted: 23 February 2020 doi:10.20944/preprints202002.0333.v1

CMORPH satellite data. CMORPH data are extracted using the coordinates location of the rain gauges.

In the second way (areal comparison) CMORPH rainfall estimation is compared with the interpolated Rg-SENAMHI rainfall stations. The Rg-SENAMHI rainfall observations are interpolated adopting method [49] and compared with the respective CMORPH rainfall estimation for LTb.

Table 1. Summary of rainfall dataset used

Data description (Reference)	Spatial and temporal resolution and coverage	Data sources	Online documentation
CMORPH (Joyce et al. 2004)	0,07275° grid, 60°S-60°N, 180°W-180°E; 30 min., 12/2002-present.	Microwave estimates from the DMSP 13, 14 and 15 (SSM/I), the NOAA-15, 16 and 17 (AMSU-B) and the TRMM (TMI) satellites are propagated by motion vectors derived from geostationary satellite infrared data.	http://www.cpc.ncep.noaa.gov/products/janowiak/cmorph_description.html.
Rain gauges (SENAMHI) (Hunziker et al. 2017)	14°S-18°S, 71°W-69°W 1964-2013	Daily reports from 34 rain-gauges were used to derive the gridded data.	(http://www.geography.unibe.ch/research/climatology_group/research_projects/decade/index_eng.html)

3.1. Statistical measures

To compare the point observed Rg-SENAMHI with CMORPH data were used following statistical indices: the linear correlation coefficient (CORR), root mean square error (RMSE) ratio, and bias.

The coefficient of determination ($\boldsymbol{R^2}$) was adopted as a main evaluation index to evaluate quantitatively the degrre of correlation between the observed and estimated precipitaton and, is a mesuare of the degree of association between two variables.; see Eq. (1).

$$\boldsymbol{R^2} = \left(\frac{\boldsymbol{n}\sum(\boldsymbol{G_i S_i}) - (\sum \boldsymbol{G_i})(\sum \boldsymbol{S_i})}{\sqrt{(\boldsymbol{n}(\sum \boldsymbol{G_i^2}) - (\sum \boldsymbol{G_i})^2)(\boldsymbol{n}(\sum \boldsymbol{S_i^2}) - (\sum \boldsymbol{S_i})^2)}} \right)^2, \quad (\mathbf{1})$$

Where $\boldsymbol{G_i}$ is Rg-SENAMHI measurements, $\boldsymbol{R^2}$ is the coefficient of determination, $\boldsymbol{S_i}$ is CMORPH satellite estimated values, and $\boldsymbol{n}$ is number of items analyzed.

Bias is a measure tendency of how CMORPH rainfall magnitude compares Rg-SENAMHI rainfall and know if over- or under- estimated. This measure establishes the ratio of the mean CMORPH rainfall estimated value to mean Rg-SENAMHI observed value; see Eq. (2).

$$\boldsymbol{bias} = \frac{\sum_{i=1}^{n} \boldsymbol{S_i}}{\sum_{i=1}^{n} \boldsymbol{G_i}}, \quad (\mathbf{2})$$

Preprints (www.preprints.org) | NOT PEER-REVIEWED | Posted: 23 February 2020 doi:10.20944/preprints202002.0333.v1

wher $\boldsymbol{G_i}$ is the rainfall value from Rg-SENAMHI and $\boldsymbol{S_i}$ is the rainfall value from the CMORPH.

RMSE measures residuals (prediction errors) between Rg-SENAMHI and CMORPH data, and through the standard deviation calculates a weighted average error. The lower the RMSE score, the closer the CMORPH represents the Rg-SENAMHI measurements; see Eq. (3).

$$\boldsymbol{RMSE} = \sqrt{\frac{\sum_{i=1}^{n}(\boldsymbol{G_i} - \boldsymbol{S_i})^2}{\boldsymbol{n}}}, \qquad (\mathbf{3})$$

where $\boldsymbol{G_i}$ is the rainfall value from Rg-SENAMHI, $\boldsymbol{S_i}$ is rainfall value obtained from the CMORPH, and $\boldsymbol{n}$ is the total data pairs analysed.

3.2. Analysis of diurnal cycle of convection

To better understand the dayli rainfall distribution in LTb. Concept of phase will be defined and thus study the characteristics of the diurnal cycle of convection during austral summer precipitation. The period of time during which the peaks of precipitation appear, due to fluctuations in global radiation, it know as diurnal cycle phase. These events are evident, usually low latitudes, in areas where solar forcing its reached maximum values. In addition, in subtropical and polar regions is influenced by topography and frontal systems, just as it is influenced during austral winter and summer. CMORPH precipitation estimate rates is in UTC (Coordinated Universal Time) and were converted for the LTS (Local Solar Time).

To better analyze CMORPH, averages were made and accumulated for the austral summer of the period from 2002 to 2013, plotting graphs and analyzing the time of occurrence of the convective events and the peak hours of precipitation along the diurnal cycle.

Seven sub-regions were selected using criteria of similarity in the seasonal rainfall regime to better understand and explain the DCC in the LTb, due to the complexity of the study area which includes islands, mountains, basins, Peruvian altiplano and the lake Titicaca. These seven sub-regions are presented in Figure 1; four of them are in the continent and three over the lake. Maps of precipitation estimates were generated for 24 hours (at a time level), to observe the diurnal cycle of precipitation for the rainy season.

4. Results

4.1. Comparison point-to-grid

The CMORPH rainfall estimates were accumulate in annual and monthly time intervals. Rg-SENAMHI data and CMORPH values extracted for the 34 stations are represented for the three standard statistical tecnhiques (Fig. 3a-c).

Figure 3a shows an strong and weak correlations between CMORPH and Rg-SENAMHI. For CMORPH, the R^2 ranges from a minimum value of -0.39 (Lagunillas-LS ws) to a maximum of 0.75 (Chuquibambilla-CH ws). Approximately 43% total Rg-SENAMHI variation is explained CMORPH data. In figure 4, we show the relationships of CMORPH with Rg-SENAMHI in the LTb. Over southeast and northern LTb, time series of CMORPH they are positively correlated with Rg-SENAMHI data, and negatively correlated in the central and southern of LTb. For some regions (e.g., Lagunillas), the correlation coefficients were statistically insignificant .

Preprints (www.preprints.org) | NOT PEER-REVIEWED | Posted: 23 February 2020 doi:10.20944/preprints202002.0333.v1

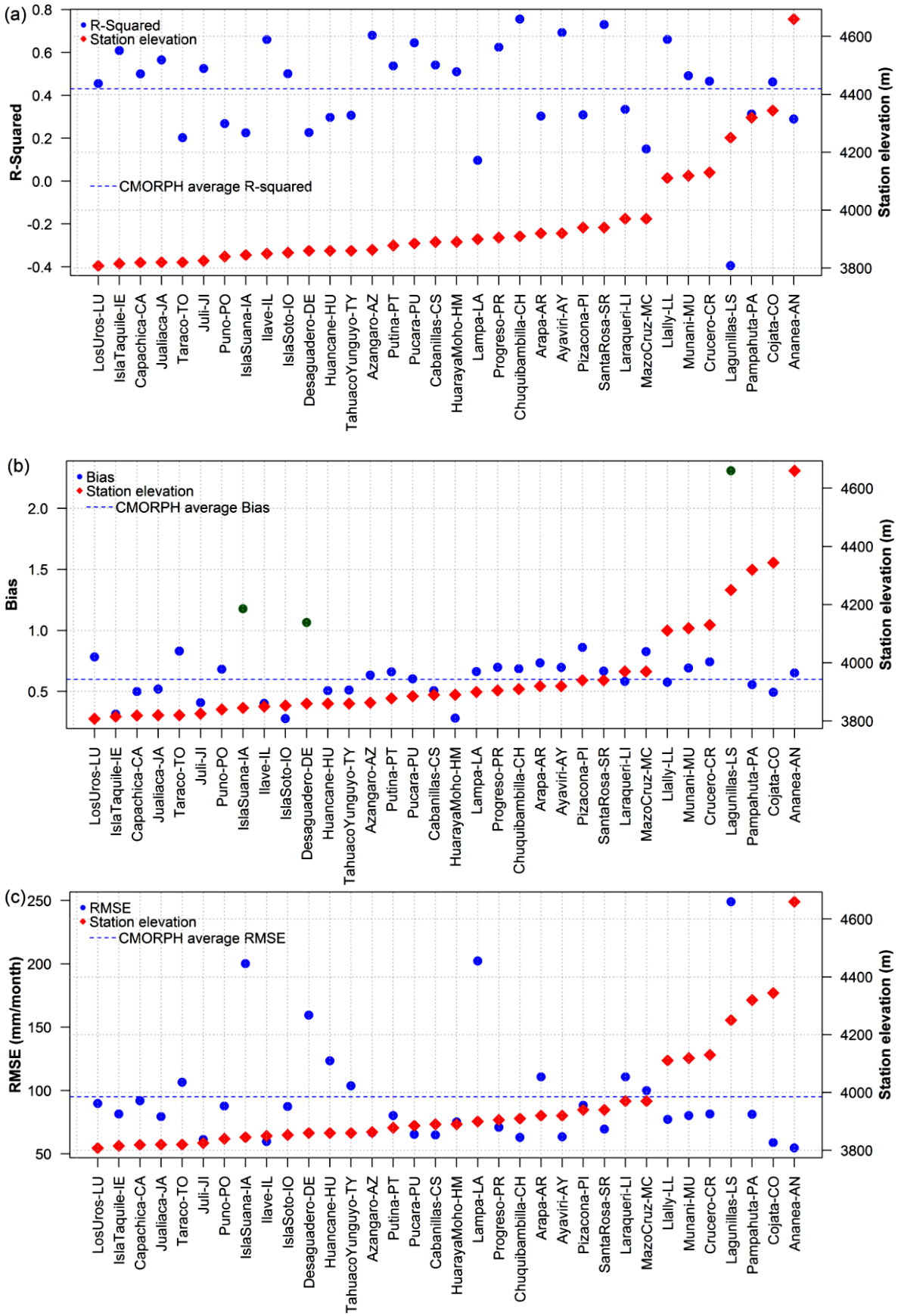

Figure 3. (a) R^2 of CMORPH compared with 34 RgSENAMHI in the LTb. **(b)** Bias de CMORPH compared with 34 Rg-SENAMHI in the LTb. **(c)** RMSE of CMORPH compared with 34 Rg-SENAMHI in the LTb. All sorted by station elevation.

Preprints (www.preprints.org) | NOT PEER-REVIEWED | Posted: 23 February 2020 doi:10.20944/preprints202002.0333.v1

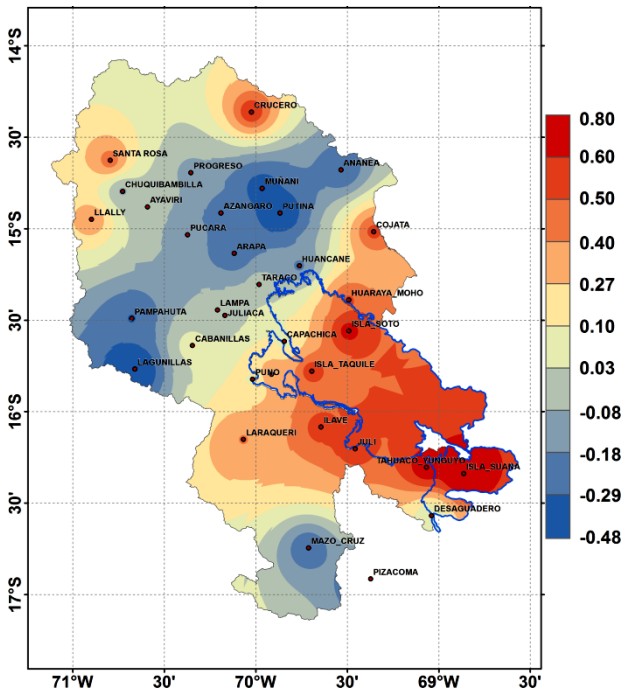

Figure 4. Pearson correlation coefficients (Pearson) of CMORPH with Rg-SENAMHI for the period 2002-13

The bias calculated (Fig. 3b) for CMORPH and Rg-SENAMHI ranges from 0.28 to 0.86. The CMORPH underestimated Rg-SENAMHI observed data; approximately, underestimate values was 60%. CMORPH overestimate 3 stations (Lagunillas-LS, Isla Suana-IA and Desaguadero-DO, marked in green circles in Fig. 5b). This stations registered average values of 150 mm of rainfall during dry season months (June, July and August), that increased the annual cumulative average (Fig. 5a). The RMSE shown in Fig. 3c present similar trends as in Fig. 3a. The RMSE shows high values (150.5 mm month^{-1}, 200.2 mm month^{-1} and 249.1 mm month^{-1}) for Lagunillas-LS, Isla Suana-IA and Desaguadero-DO stations, respectively, and a RMSE below average (95 mm month^{-1}) for others stations.

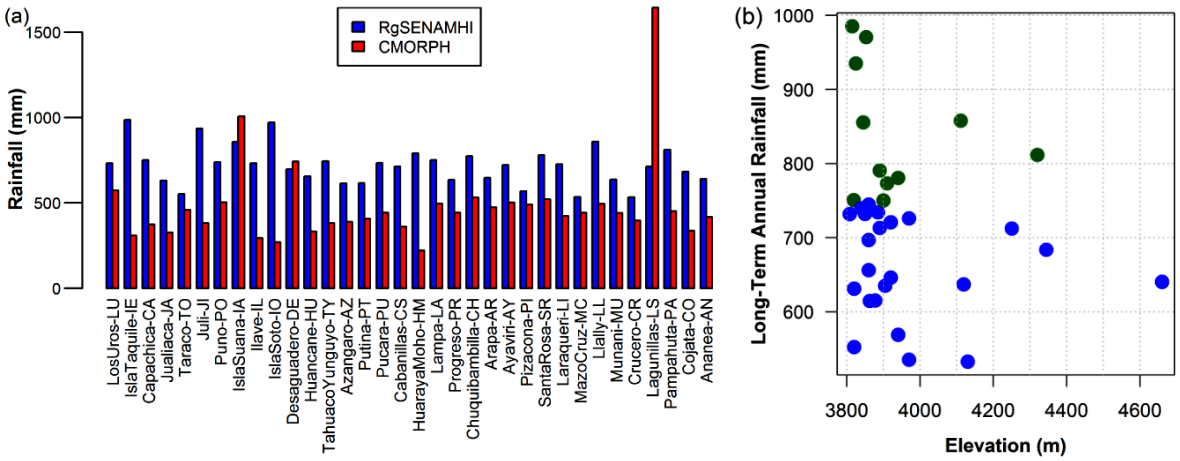

Figure 5. (a) Annual average rainfall CMORPH and Rg-SENAMHI (2002 - 2013) of selected stations in LTb. (b) Elevation vs. annual precipitation average relations over the Lake Titicaca Basin (34 weather stations and period 2002-2013).

Figure 5b shows 11 weather stations, green circles, with a better correlation coefficient and a smaller root mean square error values, due to probably affected by rains of convective origin. On the

other hand, 23 weather station (blue circles shows in figure 5b) probably affected by a combination rains fo convective and orographic origin. In consequence, stations probably affected by both orographic and convective rainfall will have a higher bias than the stations probably affected by convective precipitation only. These results agree with the findings of [50] where, 16 stations registered a higher bias, concluding that, stations located in mountain hillslope would be affected because of orographic lifting of moist air that generate rainfall, while the other stations located in the plain would be affected by convective rainfall.

4.2. Areal comparison

To make a more realistic comparison, areal Rg-SENAMHI is compared with the areal CMORPH for the LTb, through the methodology of linear multiple regression, where topography variable has been included in rainfall spatial distribution (Fig. 6a-d). Initially average annual accumulated rate of precipitation was compared. Precipitation rates distribuitions shown in figure 5a-b (period 2002-2013), derived from CMORPH and Rg-SENAMHI, respectively. CMORPH stations with values recorded in dry season shows precipitation maxima over three regions: the south, western and southwestern of LTb (Fig. 6a).

We can see that both the extend and magnitude of maximum rainfall from Rg-SENAMHI data exist mainly over Titicaca Lake (Fig. 6b). Note that over Lake Titicaca basin precipitation characteristics is non-uniform well, this is likely due to the influence of both convective and orographic precipitation, showing notable accordance with major precipitation patterns exist in these regions due to presence over Andean slopes. During the summers (December, January and February) of 2002-2013 the distributions of mean precipitation rates derived from CMORPH and Rg-SENAMHI indicate decreases from the northwest to the southeast (Fig. 6c) and from the north to the south (Fig.6d). CMORPH high temporal-spatial resolution shows Foehn effect existence over northeastern region of LTb (Fig. 6c), this was corroborated with observed data of the stations located on Chaupi Orco hillslope (Fig. 6d). Masses of moist air transporte by SALLJ (South American Low-Level jet east of the Andes), fall as precipitation on the hillslope due to mountain presence (cf. Figure 3a in Garreaud et al 2003 [28]). In this region Andean slopes acts as a natural barrier restricting the entry of moisture from Amazon basin, and consequence, there is water vapor deficiency on the other side (leeward) . These results were also obtained by Zhang et. al [51], who used satellite data from CMORPH and TRMM on the South and East Asia region. Precipitation pattern over LTb, obtained with Rg-SENAMHI data, was entire represented form CMORPH data. The southeastern and northeastern regions, precipitation patterns, were well respresented.

The areal bias computed (Fig. 7a-b), which represents the difference between CMORPH and Rg-SENMAHI, presented a high underestimation percentage of annual cumulative average rainfall (300% on average), while that for summer precipitation the areal bias underestimates by an average of 78%. The bias for CMORPH both for the annual cycle of precipitation and austra summer is not constant; it overestimates for Lagunillas by 930% and underestimates for Isla Soto by 700% (Fig. 7a). The summer precipitation bias map (Fig. 7b) indicated that the CMORPH consistently underestimates the Rg-SENAMHI; for Isla Soto and Lagunillas by 156 and 38 %, respectively.

4.3. Diurnal cycle of convection using CMORPH data

We examine the characteristics of the summer precipitation diurnal cycle in detail using the high resolution CMORPH data. Spatial distribution of DCC intensity (Fig. 8a-v) and phase of wet period rainfall (December - February) over the Titicaca Lake and its peripheral areas (period 2002 - 2013), derived from CMORPH estimates. As shown in Fig. 8, over continental areas, the precipitation peaks in the afternoon. Over the surrounding lake area, high mountain, and plateau area, maximum peaks of precipitation occur in the early evening, neverhtheless over low areas such as the lake,

Preprints (www.preprints.org) | NOT PEER-REVIEWED | Posted: 23 February 2020 doi:10.20944/preprints202002.0333.v1

surrounding and valleys, maximum precipitation values occur early morning. This is due to the Altiplano region receive greater amounts radiation during the day [52,53,54], and heterogeneous tropography play a decisive role in the convective rainfall dynamics, generating moist convection and maximum low level atmospheric instability that manifests through maximum values (peaks) of precipitation in the afternoon. The predominant southeast LTb winds propagate the thermal convection activities to northwest LTb, leading to a precipitation maximum during 16:00-17:00 LST over the surrounding terrain northwest Titicaca Lake (Fig. 8m).

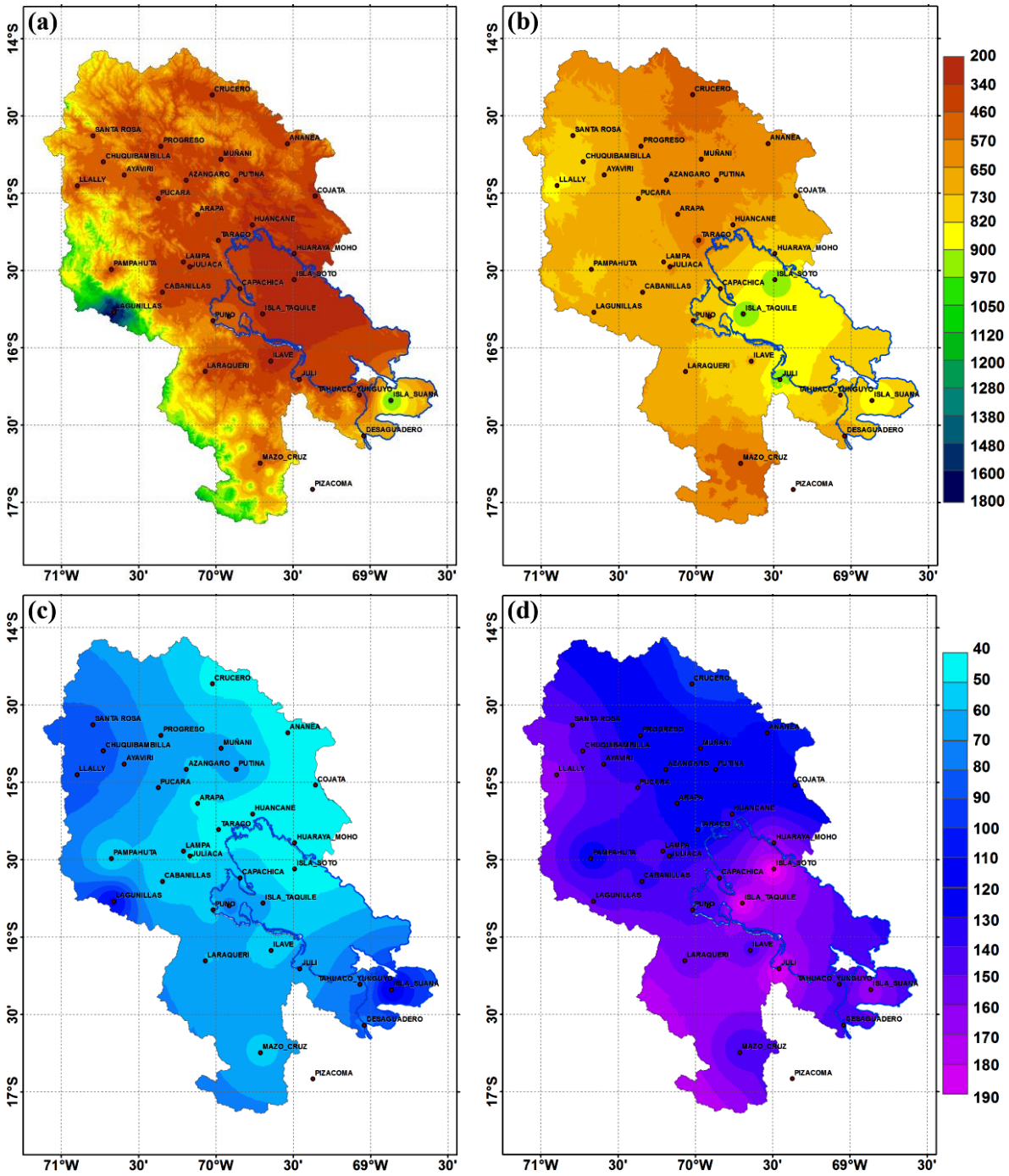

Figure 6. Spatial distribution of the annual and summer season precipitation (2002-2013): (a) CMORPH, (b) observed data. For the summer precipitation(DJF): (c) CMORPH, (d) observed data. The scale in colors represents the precipitation in millimeters (mm). Vertical axis indicates the latitudes and the horizontal axis refers to the lengths, both em degrees (°)

Preprints (www.preprints.org) | NOT PEER-REVIEWED | Posted: 23 February 2020 doi:10.20944/preprints202002.0333.v1

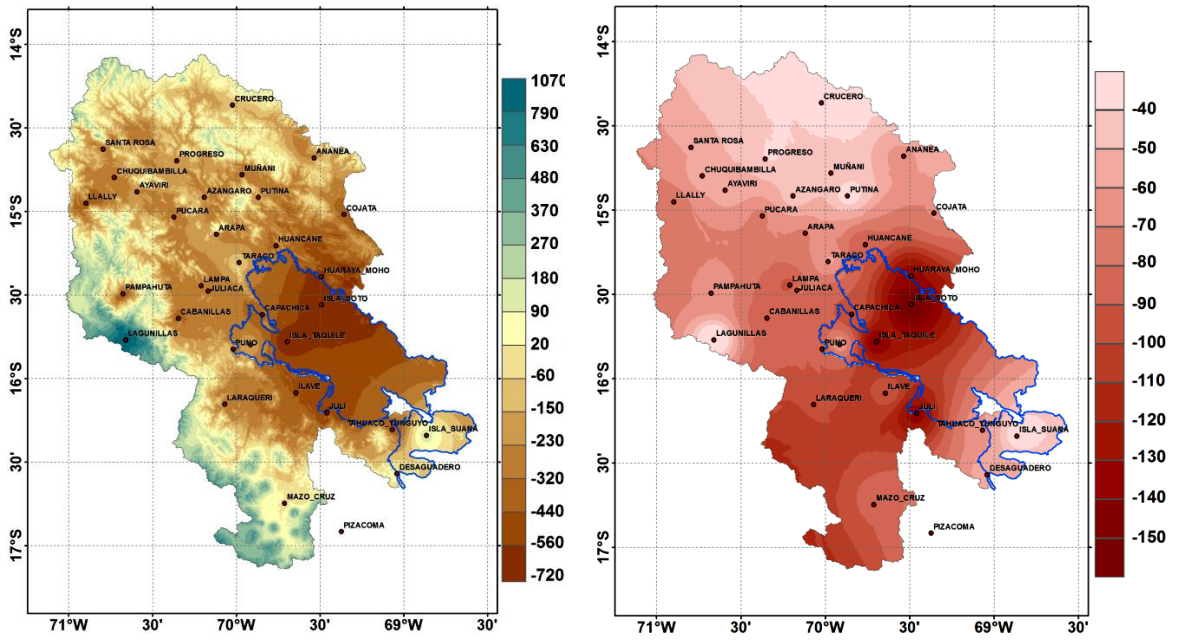

(a) (b)

Figure 7. Bias spatialization map for the annual precipitation cycle (a), and for the summer precipitation (b). Period 2002-2013. Scale in colors represents the underestimation or overestimation of CMORPH compared to RgSENAMHI.

Over the Titicaca Lake, precipitation peaks generally occurs between midnight and sunrise. The maximum precipitation usually occurs during 04:00-06:00 LTS (Fig. 8d), especially over northwest Titicaca Lake. WRF model results were compared rather favorably with observations in the SALLJEX simulations [55], that showed that the regions of preferred convergence and vertical motion are consistent with distribution pattern derived from CMORPH data. Both results are consequent with studies cited to in Section 1.

During nighttime (Fig. 8a,s,v), there is internal gravity waves propagation, due to radiative cooling over complex orography causing drainage flows, which can produce low-level convergence over the lake. With the air coming from the continent to the lake, of terrestrial breeze front is formed with upward motion on the lake. In some cases it is possible to observe clouds formation and precipitation cores estimates.

Figure 9 shows DCC average for seven selected regions in the Lake Titicaca basin (See Fig. 1 for the locations on a map) derived from CMORPH. Region 1 - Puno; Reg. 2 - Santa Rosa; Reg. 3 - Crucero; Reg. 4 - Cabanillas; Reg. 5 - Isla Suana; Reg. 6 - Arapa; and Reg. 7 - Isla Soto. In particular, in the regions 3, 5 and 7 we observed an obvious semi diurnal cycle. On the other hand, in the 1,2,4 and 6 regions, the diurnal cycle of convection is similar and the peaks occur in the afternoon period which is consistent with the previos results [5,42]. When we compared figure 9a with figure 10 (observed data) the results suggests that CMORPH can represented the diurnal phase of convective rainfall. The time of maximum peak is about 1-2 h earlier that Rg-SENAMHI-puno. It is around 18:00 LST.

This results suggests that, the main pattern of the diurnal cycle of convection is consistent with previous studies [5,14,42,43]. On the other hand, the high resolution of the CMORPH data used here, show more significant regional differences when compared to previous studies, such as a less coherent phase pattern over certain regions (Reg. 3, 5 and 7). This results suggest that, DCC main pattern is regulated by surface exchange processes over heteogeneous topography, valley breezes

Preprints (www.preprints.org) | NOT PEER-REVIEWED | Posted: 23 February 2020 doi:10.20944/preprints202002.0333.v1

and slope who play a important role on convective and orographyc processes near to the mountains [56-58].

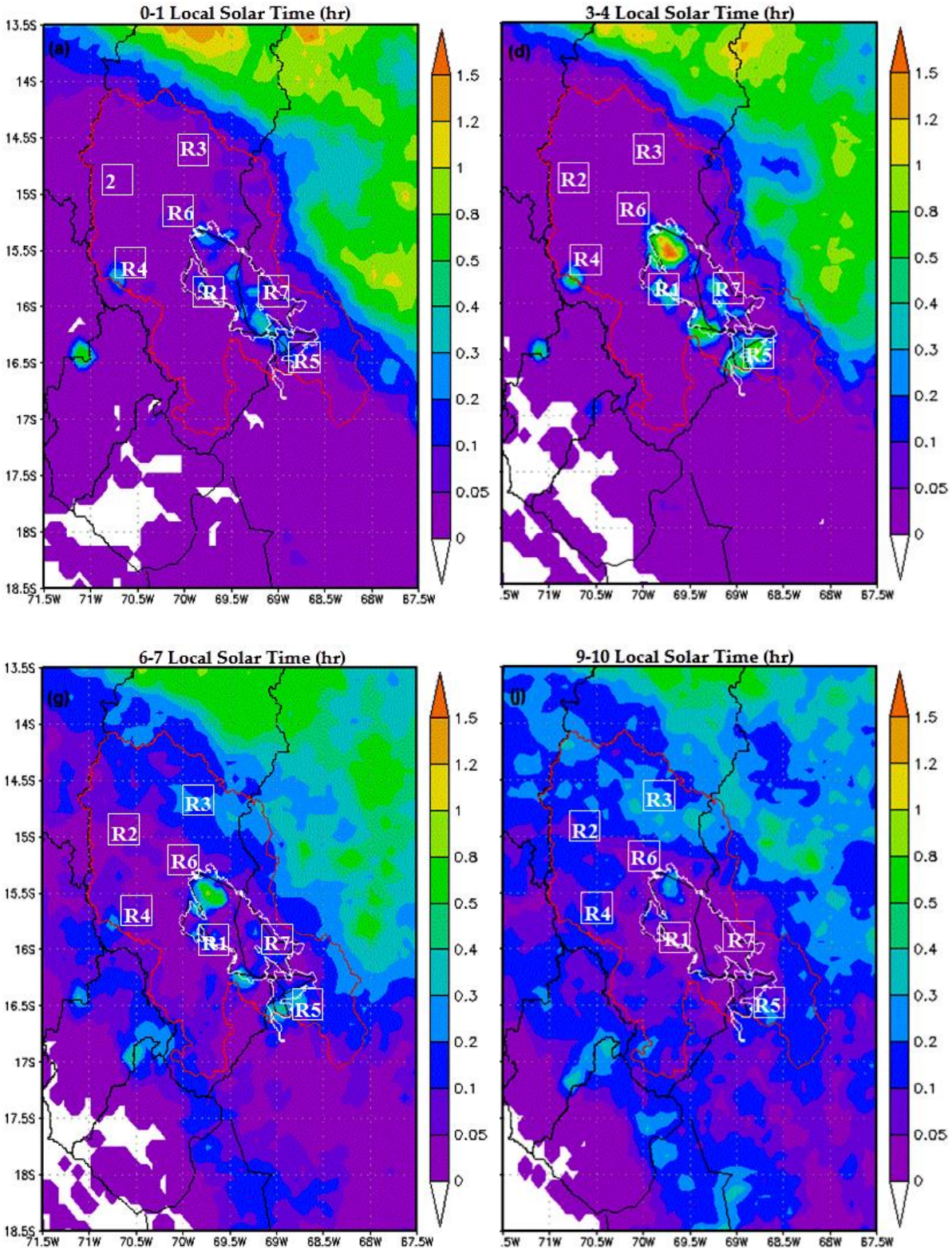

Figure 8. Spatial distribution of the average rainfall accumulation field obtained from the CMORPH data, period 2002-2013. Color scale represents precipitation in millimeters (mm/hr). DCC is represented in LST (local solar time). Vertical axis indicates the latitudes and the horizontal axis refers to the lengths, both in degrees (°). The white boxes are the regions selected for the analysis.

Preprints (www.preprints.org) | NOT PEER-REVIEWED | Posted: 23 February 2020 doi:10.20944/preprints202002.0333.v1

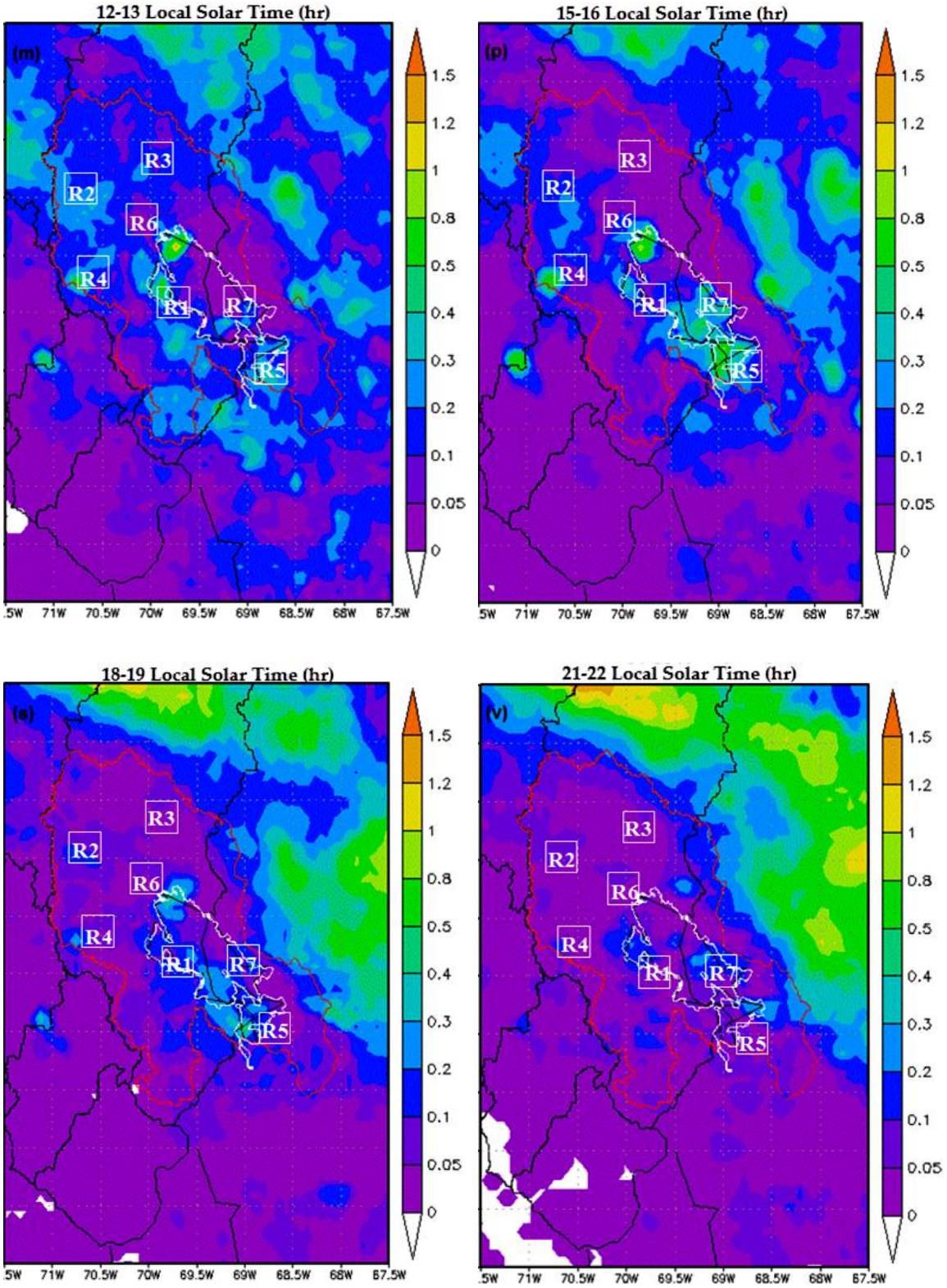

Figure 8. (continued)

The diurnal cycle configuration over Titicaca lake and its surroundings can may result by local circulation influenced for the surface energy balance (SEB) and the complex terrain. The slope mountain effects on the available radiant energy [53,54,57,58], orographic moisture blockage over the LTb, and the corresponding local advection processes impact the DCC.

Preprints (www.preprints.org) | NOT PEER-REVIEWED | Posted: 23 February 2020 doi:10.20944/preprints202002.0333.v1

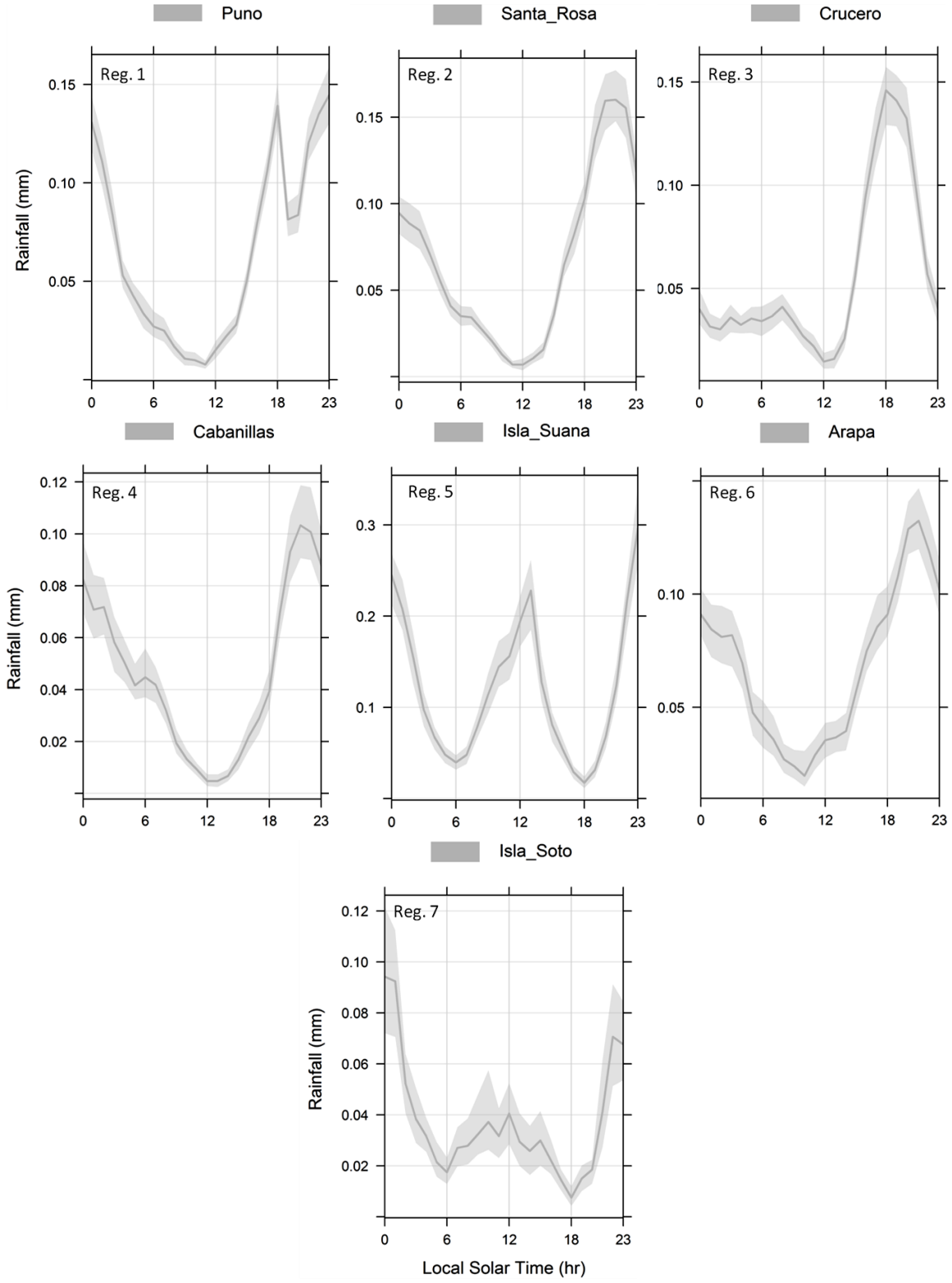

Figure 9. Graphic representation DCC for the summer season in the . CMORPH (thin gray solid line indicates 2002-2013). The diurnal cycle of convection phase (LST) is respresented in the abscissa and precipitation rate average (units: milemeters / hour) over LTb in the ordinates.

In this matter, regional water vapor conditions from Titicaca lake and other factors could affect the regional characteristics of DCC. Understand how this mechanism influence the DCC over the surrounding terrain remains to be further investigated.

Preprints (www.preprints.org) | NOT PEER-REVIEWED | Posted: 23 February 2020 doi:10.20944/preprints202002.0333.v1

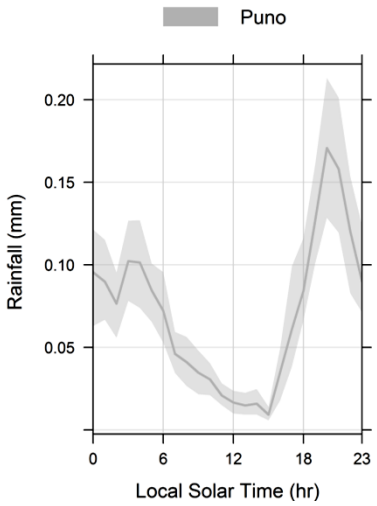

Figure 10. Mean diurnal cycle of summer precipitation at automatic weather station (Puno). Rg-SENAMHI-puno (thin gray solid line indicates 2014-2018). The diurnal cycle of convection phase (LST) is respresented in the abscissa and precipitation rate average (units: milemeters / hour) over LTb in the ordinates..

5. Conclusions

Currently, the accuracy of rainfall estimates is very import for the expansion and maintenance of the agricultural frontier, water security of LTb communities, and to reduce natural desasters directly related to droughts and floods [1,34,56,59]. In this study, our objective was to evaluate CMORPH rainfall estimates over Lake Titicaca basin. The river Desaguadero is the main beneficiary with the waters collected by this basin. The evaluation is carried out on several time scales (annual, seasonal and hourly) and with resolution (8 x 8 km^2) for the period between January 2002 and December 2013 obtained from CMORPH, and the evaluation was carred out based on 34 rain gauges distributed in our study area. To examine CMORPH data accuracy, graphic techniques and statistical measures were used. When interpreting rain maps generated with surface station data, special care was taken in the regions that have few or no rain gauges , especially over Southwestern LTb. The main conclusions will be made based on the results presented as follows:

1. CMORPH estimates exhibit remarkable agreement with regard precipitation patterns observed with Rg-SENAMHI, and achieved to capture daily rainfall frequency better that rainfall amounts over the LTb. Maximum precipitation peaks can be appreciated in two well-marked regions: Over Titicaca Lake and surrounding terrain. It should be noted that, both extend and magnitude of maximum precipitation form CMORPH data underestimate Rg-SENAMHI precipitation data. On the other hand, CMORPH precipitation estimates underestimate in most LTb regions, except in some regions (e.g., Lagunillas, Isla Suana and Desaguaderos stations) were rainfall is overestimated.

2. Rainfall distribution over our interest area shown regional differences that are seen in the convective diurnal cycles. Over low regions such as the valleys (near to lake) and Titicac lake, it maximum peaks rainfall around midnight and ends to early morning. The results show that DCC its very related by surface exchange processes and local circulation resulting from solar radiation and heterogeneous topography.

3. The bias underestimation is observed over most the LTb areas and overerestimation (e.g., Lagunillas, Isla Suana and Desaguadero stations). The total bias increases/decreases near mountais and attaining maximum value when approaching to lake respectively [4,5]. In addition, high spatial and temporal resolution CMORPH data can captured regional details (e.g., Isla Suana) which show a less coherent phase pattern that the others stations.

4. CMORPH and Rg-SENAMHI precipitation amounts show moderate to weak correlations (59 % and 41 %) respectively. Higher correlation are observed over the lake (>0.6). Based on the period and study area, we observed that CMORPH accuracy over lake Titicac basin shows large spatial-temporal variability and exist there a distinct difference between Rg-SENAMHI and CMORPH accurary [4,5]. On the other hand, a spatial-temporal variable bias correction should be made to the CMORPH product in order to assess the implications of these adjustments and their application in water resources over the Lake Titicaca basin [60].

Acknowledgments: The present work was the result of the master's thesis financed by Capes (Coordination of Improvement of Higher Level Personnel), foundation of the Ministry of Education of Brazil.

Author Contributions: Eleazar Chuchón and Augusto Pereira analyzed the data; Augusto Pereira contributed materials and analysis tools; Eleazar Chuchón wrote the article.

Conflicts of Interest: "The authors declare no conflict of interest." and "The founding sponsors had no role in the design of the study; in the collection, analyses, or interpretation of data; in the writing of the manuscript, and in the decision to publish the results".

Abbreviations
The following abbreviations are used in this manuscript:

LTb: Lake Titicaca Basin
CMORPH: CPC MORPHing technique
LST: Local Solar Time
RgSENAMHI: Rain gauge SENAMHI

References

1. Canedo, C.; Pillco R.Z.; Berndtsson R.: Role of Hydrological Studies for the Develompent of the TDPS System. Water, 2016, 8, 144, https://doi.org/10.3390/w8040144
2. Li, J.; Heap, A.D.: Spatial Interpolation Methods: A Review for Environmental Scientists, 2008, http://www.ga.gov.au/corporate_data/68229/Rec2008_023.pdf
3. Scheel, M.L.M.; Rohrer, M.; Huggel, C.; Santos Villar, D.; Silvestre, E.; Huffman, G.J.: Evaluation of TRMM Multi-satellite Precipitation Analysis (TMPA) performance inthe Central Andes region and its dependency on spatial and temporal resolution.*Hydrol. Earth Syst. Sci*., 2011, 15, 2649–2663. http://dx.doi.org/10.5194/hess-15-2649-2011
4. Haile, A. T.; Yan, T.; Habib, E.: Accuracy of the CMORPH satellite-rainfall product over Lake Tana Basin in Eastern Africa. *SciencieDirect, Atmospheric Research*, 2015, Vol. 163, 177-187, https://doi.org/10.1016/j.atmosres.2014.11.011
5. Zhang, X.-X.; Bi, X.-Q.; Kong, X.-H. Observed Diurnal Cycle of Summer Precipitation over South Asia and East Asia Based on CMORPH and TRMM Satellite Data. *Atmos Ocean Sci Lett* (8):2015, 201–7, http://doi.org/10.3878/AOSL20150010
6. Dinku, T.; Connor S.J.; Ceccato, P.: Comparation of CMORPH and TRMM-3B42 over Mountainous Regions of Africa and South America, In: *Gebremichael M.; Hossain, F.; (eds) Satellite Rainfall Applications for Surface Hydrology, Springer, Dordrecht*, 2009, http://doi.org/10.1007/978-90481-2915-7_11
7. Pereira, F.A.J.; Carbone, R.E.; Janowiak, J.E.; Arkin, P.; Joyce, R.; Hallak, R.; Ramos, C.G.M.: Satellite rainfall estimates over South America-Possible applicability to the water management of large watersheds. *Journal of the American Water Resources Associations*, 2010, 46, 344-360, http://doi.org/10.1111/j.1752-1688.2009.00406.x
8. Pereira, F.A.J.; Vemado, F.; Vemado, G.; Gomes,V.R.F.A.; Do Carmo, G.L.; Irineu, C.R.; Dos Santos, C.C.; Sampaio, L.E.S.; Fischer, G.M.; Tadashi, O.A.; Zaine, J.E.; Da Silva, C.L.E.; Filho, O.A.; Mazo, D.F.; Dos Santos, A.C.: A Step towards Integrating CMORPH Precipitation Estimation with Rain Gauge Measurements, *Hindawi, Advances in Meteorology*, 2018, ID:2095304, 24, http://doi.org/10.1155/2018/2095304.
9. Ruiz, J.J.: Evaluation of different methodologies for precipitation estimates calibration-cmorph-over South America, Rev. Bras. Meteorol.,2009, Vol. 24, 4, http://dx.doi.org/10.1590/S0102-77862009000400009

10. Sapriano, M.R.P.; Arkin, P.A.: An Intercomparison and Validation of High-Resolution Satellite Precipitation Estimates with 3-Hourly Gauge Data, *Amer. Meteor. Soc., 2019, Journal of Hydrometeorology*, Vol. 10, 149-166, http://doi.org/10.1175/2008JHM1052.1
11. Dinku, T.; Chidzambwa, S.; Ceccato, P.; Connor, S.J.; Ropelewski, C.F.: Validation of high-resolution satellite rainfall products over complex terrain, *International Journal of Remote Sensing*, 2008, 29:14, 4097-4110, https://doi.org/10.1080/01431160701772526
12. Satgé, F.; Bonnet, M.-P.; Gosset, M.; Molina, J.; Yuque, L.W.H.; Pillco, Z.R.;Timouk, F.; Garnier, J.: Assessment of satellite rainfall products over the Andean plateau, SciencieDirect, Atmospheric Research, 2016, 167, 1-14, http://dx.doi.org/10.1016/j.atmostres.2015.07.012.
13. Satgé, F.; Ruelland, D.; Bonnet, M.-P.; Gosset, M.; Molina, J.; Pillco, Z.R.: Consistency of satellite-based precipitation products in space and over time compared with gauge observations and snow-hydrological modelling in the Lake Titicaca region, *Hydrol. Earth Syst. Sci.*, 2019, 23, 595-619, https://doi.org/10.5194/hess-23-595-2019
14. Dai, A.; Lin, X.; Hsu, K.-L.: The frequency, intensity, and diurnal cycle of precipitation in surface and satellite observations over low- and mid-latitudes, *Clim Dyn*, 2007, 29:727-744, http://doi.org/10.1007/s00382-007-0260-y
15. Janowiak, J.E.; Arkin, P.A.; Morrissey, M.: An examination of the diurnal cycle in oceanic tropical rainfall using satellite and in situ data. *Mon Weather*, 1994, Rev 122:2296–2311, https://doi.org/10.1175/1520-0493(1994)122<2296:AEOTDC>2.0.CO;2
16. Chang, A.T.C.; Chiu, L.S.; Yang, G.: Diurnal cycle of oceanic precipitation from SSM/I data. *Mon Weather*, 1995, Rev 123:3371–3380, https://doi.org/10.1175/1520-0493(1995)123<3371:DCOOPF>2.0.CO;2.
17. Sorooshian, S.; Gao, X.; Maddox, R.A.; Hon, Y.; Imam, B.: Diurnal variability of tropical rainfall retrieved from combined GOES and TRMM satellite information. *J. Clim*, 2002, 15:983–1001, https://doi.org/10.1175/1520-0442(2002)015<0983:DVOTRR>2.0.CO;2
18. Nesbitt, S.W.; Zipser, E.J.; The diurnal cycle of rainfall and convective intensity according to three years of TRMM measurements. *J. Clim*, 2003, 16:1456–1475.
19. Bowman, K.P.; Collier, J.C.; North, G.R.; Wu, Q.Y.; Ha, E.H,; Hardin, J.: Diurnal cycle of tropical precipitation in Tropical Rainfall Measuring Mission (TRMM) satellite and ocean buoy rain gauge data. *J, Geophys*, 2005, Res 110:D21104, http://org.doi/21110.21029/22005JD005763
20. Hong, Y.; Hsu, K.L.; Sorooshian, S.; Gao, X.G.: Improved representation of diurnal variability of rainfall retrieved from the Tropical Rainfall Measurement Mission Microwave Imager adjusted Precipitation Estimation From Remotely Sensed Information Using Artificial Neural Networks (PERSIANN) system. *J, Geophys*, 2005, Res 110:D06102 https://doi.org/10.1029/2004JD005301
21. Yang, S.; Smith, E.A.; Mechanisms for diurnal variability of global tropical rainfall observed from TRMM. *J, Climate*, 2006, 19:5190–5226, https://doi.org/10.1175/JCLI3883.1
22. Hur, J.; Srivatsan, V.R.; Ngoc, S.N.; Shie-Yui, L.: Evaluation of High-Resolution Satellite rainfall data over Singapure, ScienceDirect, *Procedia Engineering*, 2016, 154, 158-167, doi:10.1016/j.proeng.2016.07.437.
23. Shang, H.; Letu, H.; Nakajima, T.Y.; Wang, Z.; Ma, R.; Wang, T.; Lei, Y.; Ji, D.; Li, S.; Shi, J.: Diurnal cycle and seasonal variation of cloud cover the Tibetan Plateau as determined from Himawari-8 new-generation geostationary satellite data, Scientific Reports, 2018, 8:1105, doi:10.1038/s41598-018-19431-w.
24. Wang, G.; Zhang, P.; Liang, L.; Zhang, S.: Evaluation of precipitation from CMORPH, GPCP-2, TRMM 3B43, GPCC, and ITPCAS with ground-based measurements in the Qinling-Daba Mountains, China, PLoS ONE, 2017, 12(10): e0185147, https:// doi.org/10.1371/journal.pone.0185147.
25. Dai, A.: Global Precipitation and Thunderstorm Frequencies. Part I: Seasonal and Interannual Variations, *Journal of Climate*, 2000, Vol. 14, 1092-1111, https://doi.org/10.1175/1520-0442(2001)014
26. Du, Y.; Rotunno, R.: Diurnal Cycle of Rainfall and Winds near the South Coast of China, *American Meteorology Society*, 2018, Vol. 75, 2065-2082, https://doi.org/10.1175/JAS-D-17-0397.1.
27. Watters, D.; Battaglia, A.: The Summertime Diurnal Cycle of Precipitation Derived from IMERG, *Remote Sens*, 2019, 11,1781, doi:10.390/rs11151781.
28. Garreaud, R.; Vuille, M.; Clement, A.: The climate of the Altiplano: observed current conditions and mechanisms of past changes.. *Palaeogeography, Palaeoclimatology, Palaeoecology*, 2003, **194**, pp. 5–22, doi:10.1016/S0031-0182(03)00269-4
29. Garreaud, R.: Intraseasonal Variability of Misture and Rainfall over the South American Altiplano, *Amer. Meteor. Soc.*,2000, Vol. 128, 3337-3346.

30. Villue, M; Keimig, F.: Interannual Variability of Summertime Convective Cloudiness and Precipitation in the Central Derived from ISCCP-B3 Data, *Journal of Climate*, 2004, Vol. 17, pp. 3334-3348.
31. OEA (Organización de los Estados Americanos)/ PNUMA (Programa de las Naciones Unidas para el Medio Ambiente), *Diagnóstico Ambiental del Sistema Titicaca-Desaguadero-Poopó-Salar de Copaisa (Sistema TDPS)*, 1996, Bolivia-Perú, p.192 (Washington, DC:OEA).
32. Heidinger, H.; Yarlequé, C.; Posadas, A.; Quiroz, R.: TRMM rainfall correction over the Andean Plateau using wavelet multi-resolution analysis, International Journal of Remote Sensing, 2012, 33:14, 4583-4602, https://doi.org/10.1080/01431161.2011.652315
33. Torre-Batlló, J.; Martí-Cardona, B.; Pillco-Zolá, R.: Mapping long-term evapotranspiration losses in the catchment of the shrinking Lake Poopó, *Hydrology and Earth System Sciences*, 2019, Preprint. Discussion started: 28 May 2019, https://doi.org/10.5194/hess-2019-187.
34. Zamuriano, M.; Martynov, A.; Panziera, L.; Bronnimann, S.: Characteristics of a Hailstorm over the Andean La Paz Valley, *Nat. Hazards Earth Syst. Sci*., 2019, https://doi.org/10.5194/nhess-2019-27
35. Blacutt, L.A.; Herdies, D.L.; De Gonçalves, L.G.G.; Vila, D.A.; Andrade, M.: Precipitation comparison for the CFSR, MERRA, TRMM3B42 and Combined Scheme datasets in Bolivia, *ScienceDirect, Atmospheric Research*, 2015, 163, 117-131, http://dx.doi.org/10.1016/j.atmosres.2015.02.002
36. Gebere, S.B.; Alamirew, T.; Merkel, B.J.: Performance of High Resolution Satellite Rainfall Products over Data Scarse Parts of Eastern Ethiopia, Remote Sens., 2015, 7, 11639-11663, doi:10.3390/rs70911639
37. Joyce, R.J.; Janowiak, J.E.; Arkin, P.A.; Xie, P.: CMORPH: A Method that Produces Global Precipitation Estimates from Passive Microware and Infrared Data at High Spatial and Temporal Resolution, Journal of Hydrometeorology, 2004, 5, 487-503.
38. Joice, R.J.; Xie, P.; Yarosh, Y.; Janowiak, J.E.; Arkin, P.A.: CMORPH: A "Morphing" Approach for High Resolution Precipitation Product Generation, 2009, *Satellite Rainfall Applications for surface Hydrology*, doi 10.1007/978-90-481-2915-7_2.
39. Rais, A.F.; Yunita, R.: Main Diurnal Cycle Pattern of Rainfall in East Java, AIP Conference Proceedings 2017,1876, 020057, https://doi.org/10.1063/1.4994460.
40. Zhu, L.; Meng, Z.; Zhang, F.; Markowski, P.M.; The influence of sea- and land-breeze circulations on the diurna variability in preciptation over a tropical island, *Atmos. Chem, Phys*, 2017, 17, 13213-13232, https://doi.org/10.5194/acp-17-13213-2017.
41. Hussain, Y.; Satgé, H.; Hussain, M.B.; Martinez-Carvajal, H.; Bonnet, M.-P.; Cárdenas-Soto, M.; Roig, H.Ll.; Akther, G.: Performance of CMOPRH, TMPA, and PERSIANN rainfall datasets oven plain, mountainous, and glacial regions of Pakistan, *Theor. Appl. Climatol*, 2018, 131:1119-1132, DOI 10.1007/s00704-016-2027-z
42. Janowiak, J.E.; Kousky, V.E.; Joyce, R.J.; Diurnal cycle of precipitation determined from the CMORPH high spatial and temporal resolution global precipitation analyses, Journal of Geophysical Research, 2005, Vol. 110, D23105, doi:10.1029/2005JD006156.
43. Giles, J.A.; Ruscia, R.C.; Menéndez, C.G.: The diurnal cycle of precipitation over South America represented by five gridded datasets, *International Journa of Climatology*, 2019, 1-19, DOI: 10.1002/joc.6229.
44. Trinh-Tuan, L.; Matsumoto, J.; Ngo-Duc, T.; Nodzu, M.I.; Inoue, T.: Evaluation of satellite precipitation products over Central Vietnan, *Progress in Earth and Planetary Science*, 2019, 6:54, https://doi.org/10.1186/s40645-019-0297-7.
45. TDPS: Climatología del sistema de los lagos Titicaca, Desaguadero,Poopó y Salares Coipasa y Uyuni (TDPS), Comisión de comu-nidades de europeas, Repúblicas del Perú y Bolivia, conveniosALA/86/03 y ALA/87/23, LP, Bolivia, 1993.
46. Revollo, M.M.; Management issues in the Lake Titicaca and Lake Poopo System: Importance of developing a water budget. *Lake and reservoirs,* 2001, Vol. 6, issue 3, 225-229, https://doi.org/10.1046/j.1440-1770.2001.00151.x
47. Roche, M.A.; Bourges, J.; Cortes, J.; Mattos, R. Climatology and hydrology of the Lake Titicaca basin. in: Lake Titicaca. A syntl1esis of Limnological Knowleage, *Monographiae Biologicae 68, Kluwer Academic Publishers*, (*C. Dejoux & A. litis eds*.): 1992, 63-88.
48. Hunziker, S.; Gubler, S.; Calle, J.; Moreno, I.; Andrade, M.; Ve-larde, F.; Ticona, L.; Carrasco, G.; Castellón, Y.; Oria, C.; Croci-Maspoli, M.; Konzelmann, T.; Rohrer, M.; and Brönnimann, S.: Identifying, attributing, and overcoming common data quality is-sues of manned station observations, *Int. J. Climatol*., 2017,37, 4131–4145, https://doi.org/10.1002/joc.5037.

49. Quevedo, K.; Sánchez, K.: Comparison of two interpolation methods to estimate air temperature applying geostatistical techniques, *Revista Peruana Geo-Atmosférica RPGA*, 2009, (1), 90-107.
50. Worqlul, A.W.; Maathuis, A.; Adem, A.A.; Demissie, S.S.; Langan, S.; Steenhuis, T.S.: Comparison of rainfall estimations by TRMM 3B42, MPEG and CFSR with ground-observed data for the Lake Tana basin in Ethiopia. *Hydrol. Earth Syst. Sci*., 2014, 18,4871-4881, doi:10.5194/hess-18-4871-2014
51. Zhang, Ch.; Chen, X.; Shao, Hua.; Chen, S.; Liu, T.; Chen, Ch.; Ding Q.; Du, H.: Evaluation and Intercomparison of High-Resolution Satellite Precipitation-GPM, TRMM, and CMORPH in the Tianshan Mountain Area, *Remote sens*, 2018,10,1543, doi:10.3390/rs10101543
52. Budyko, M.I.: Climate and life. *International Geophysics Series*, 1974, Vol 18, D.H. Miller Ed., Academic Press, 508 pp.
53. Kato, S.; Loeb, N.G.; Rosse, F.G.; Doelling, D.R.; Rutan, D.A.; Caldwell, T.E.; Yu, L.; Weller, R.A.: Surface irradiances consistent with CERES-derived top-of-atmosphere shortwave and longwave irradiances, *Journal Climate*, 2013, 26, 2719-2740, doi: 10.1175/JCLI-D-12-00436.1.
54. Gálvez, J.M.; Douglas, M.W.: Modulation of rainfall by Lake Titicaca using the WRF Model, *Proceedings of 8 ICSHMO*, 2006, 745-752.
55. Zaratti, F.; Forno, R.N.; García, J.F.: Erythemally weighted UV variations at two high-altitude locations, Journal of Geophysical Research, 2003, Vol. 108, doi:10.1029/2001JD000918.
56. Canedo, R.C.; Hochrainer-Stigler, S.; Pflug, G.; Condori, B.; Berndtsson, R.: Early warning and drought risk assessment for the Bolivian Altiplano agriculture using high resolution satellite imagery data, *Nat. Hazards Earth Syst. Sci*., 2018, Discuss., https://doi.org/10.5194/nhess-2018-133.
57. Kirshbaum, D. J.; Adler, B.; Kalthoff, N.; Barthlott, C.; Serafin, S.: Moist Orographic Convection: Physical Mechanisms and Links to Surface-Exchange Processes. *Atmosphere*, 2018,9,80, Review, doi: 10.3390/atmos9030080.
58. Serafin, S.; Adler B.; Cuxart, J.; De Wekker, S. F. J.; Gohm, A.; Grisogono, B.; Kalthoff, N.; Kirshbaum, D. J.; Rotach, M. W.; Schimdli, J.; Stiperski, I.; Vecenaj, Z.; Zardi, D.: Exchange Processes in the Atmospheric Boundary Layer Over Mountains Terrain, Atmosphere, 2018,9,102, Review, doi: 10.3390/atmos9030102
59. Canedo, R.C.; Hochrainer -Stigler, S.; Pflug, G.; Condori, B.; Berndtsson, R.: Drought risk in the Bolivian Altiplano associated with El Niño Southern Oscillation using satellite imagery data, *Nat. Hazards Earth Syst. Sci.*, 2019, Discuss., https://doi.org/10.5194/nhess-2018-403.
60. Pereira, F.A.J.; Vemado, F.; Vemado, G.; Vieria, R.A.G.; Do-Carmo, G.L.; Irineu, C.R.; Dos-Santos, C.C.; Tadashi, O.A.; Zaine, J.E.; Da-Silva, C.L.E.; Filho, O.A.; D'Affonseca, F.M.; Dos-Santos, A.C.: A Step towards Integrating CMORPH Precipitation Estimation with Rain Gauge Measurements, *Advances in Meteorology*, 2018, ID 2095304, pp 24, https://doi.org/10.1155/2018/2095304.